IEEE Access
Multidisciplinary ⋮ Rapid Review ⋮ Open Access Journal

Received December 29, 2020, accepted January 7, 2021, date of publication January 11, 2021, date of current version January 21, 2021.

Digital Object Identifier 10.1109/ACCESS.2021.3050559

A Fast Two-Dimensional Velocity Estimation Method for Multi-Channel UWB SAR

TONGXIN DANG[1] AND YIN XIANG[2]

[1]School of Data and Target Engineering, PLA Strategic Support Force Information Engineering University, Zhengzhou 450002, China
[2]Beijing Institute of Technology Chongqing Innovation Center, Chongqing 401120, China

Corresponding author: Yin Xiang (xy_overlimit@sina.cn)

This work was supported in part by the National Natural Science Foundation of China under Grant 61971039.

ABSTRACT Moving target detection in ultra-wideband synthetic aperture radar (UWB SAR) has to accumulate target energy with long integration time to improve the probability of target detection. The traditional detection and parameters estimation algorithms usually rely on parameter searching, leading to a heavy computing burden. In this paper, a fast two-dimensional velocity estimation method of moving target for multi-channel UWB SAR is proposed. The method processes the multi-channel data separately to realize the target's coherent accumulation and one-dimensional velocity estimation. Then the multi-channel signals are processed jointly to realize the two-dimensional velocity estimation. Specifically, for each channel, the second-order keystone transform is used to correct the range curvature. The symmetric autocorrelation function in the range-frequency domain is used to accumulate the moving-target energy, achieving the target detection and target's azimuth signal extraction. Next, considering the long integration time, the azimuth signal is processed by the non-uniform cubic phase function (NUCPF) based on the fourth-order phase signal to estimate the relative velocity. The azimuth signal is transformed into the Doppler domain for multi-channel data, and the interferometric signal is calculated. The phase generated by the interferometric signal is related to the radial velocity of the target. Thus, the two-dimensional velocity of the target is obtained. Finally, the effectiveness of the algorithm is verified by simulation experiments.

INDEX TERMS Moving target detection, parameters estimation, ultra-wideband synthetic aperture radar (UWB SAR), keystone transform, symmetric autocorrelation function, non-uniform cubic phase function.

I. INTRODUCTION

Low-frequency ultra-wideband synthetic aperture radar (UWB SAR) is an imaging radar that combines UWB technology and synthetic aperture technology. It has the characteristics of large beam angle and large relative bandwidth and can obtain high resolution in azimuth and range. Compared with the wideband SAR system, the outstanding advantage of low-frequency UWB SAR is that it has a strong ''perspective'' ability and can detect targets hidden in the forest [1]. At present, there are several successful UWB SAR experimental systems, including Coherent All Radio Band Sensing (CARABAS)-II operating in VHF band, LORA operating in VHF (20 $\sim$ 90 MHz) and UHF (200 $\sim$ 800 MHz), P-3 operating in VHF / UHF band with 515 MHz bandwidth. Considering the excellent ''perspective'' ability of UWB SAR, researchers have begun to apply it to moving target detection.

The associate editor coordinating the review of this manuscript and approving it for publication was Yanbo Chen.

For UWB SAR moving target detection, the moving target will produce serious displacement and defocus in the SAR image due to the long integration time. Therefore, a series of moving target focusing detection algorithms are proposed. Reference [2], [3] proposed a method that combines back-projection (BP) imaging processing with moving target detection. The BP function of moving target focusing imaging is determined by the relative speed of the target. Through the search algorithm, the relative motion speed that can maximize the target's output energy is obtained, and then target detection is realized. The experiments of LORA and CARSBAS-II verified the feasibility of the algorithm [4], [5]. Considering that the algorithm uses the blind hypothesis algorithm to estimate the relative velocity, the step size after parameter discretization must compromise between the speed measurement accuracy and the computational complexity [6].

In order to reduce the computational complexity, different parameter search strategies and frequency domain imaging algorithms are proposed. In reference [7], [8], an iterative relative velocity estimation method is proposed, which uses the

phase information of the moving target after BP processing to estimate its relative velocity, which is used for image processing. Then, the relative velocity is estimated again in the results, and the estimation accuracy is increased in the iterative process. However, this algorithm requires a higher signal-to-noise ratio (SNR) and the estimation accuracy is inferior to the parameter searching algorithm. In addition, in order to avoid the large amount of calculation brought by BP imaging, moving target detection algorithms based on different frequency-domain focusing methods are proposed, including range migration algorithm (RMA) [9], UWB chirp scaling algorithm [10], [11], local BP focusing algorithm [12], [13]. These algorithms can be used for civil traffic monitoring and can realize multiple moving target detection. When the target motion direction is known, velocity estimation and imaging can be achieved. However, the frequency domain focusing algorithms have the fixed pixel spacing in SAR images, while the BP algorithm can adjust it. It implies that the BP algorithm can realize a higher resolution in a large accumulation angle. That is, it has better focusing performance [14]. In order to retain the advantages of the BP algorithm and reduce the amount of computation, fast BP algorithms, such as PBP and FFBP, are applied to focus the moving target [15].

In addition, moving target in UWB SAR faces the problems of serious range walk and range curvature. Literature [16] proposed to use the first-order keystone transform to correct the range walk of SAR target, the energy balance filtering method to estimate and compensate the Doppler center, and the second-order keystone transform to correct the range curvature.

The above algorithms are applied for a single channel system and only estimates the relative velocity. In order to extend the application of UWB SAR in moving target detection, it is necessary to study the moving target detection of multi-aperture/channel UWB SAR system. Soumekh from Lincoln Laboratory proposed to carry two radar on the plane along the flight direction to detect the stationary and moving targets covered by leaves [17]. In addition, literature [18] demonstrated the feasibility of moving target detection using multistatic UWB SAR systems with different antennas on the same platform. In reference [19], two symmetrical sub apertures are used for SAR imaging, respectively, and the position difference of moving target in two SAR images is used to realize target detection and parameter estimation.

Combining UWB SAR with multi-channel moving target detection technology, a series of detection algorithms have emerged. The displaced phase center antenna (DPCA) is combined with the focusing detection method to eliminate the interference and detect the targets with the relative speed close to or equal to the platform speed [20], [21]. Also, along-track interferometry (ATI) can be used in multi-channel UWB SAR, which obtains the radial velocity according to the defocus target phase after BP processing and estimates the azimuth velocity by searching the maximum output of RMA with different velocity parameters [22], [23]. In addition, combining sparse array in UWB SAR with space-time adaptive processing (STAP) can solve the problem of angle ambiguity [24].

However, all of the above methods need to search parameters to achieve the moving target focusing, making it difficult to achieve real-time processing. In order to avoid parameter searching under the longer aperture time of UWB SAR, a fast two-dimensional velocity estimation method of moving target for multi-channel SAR is proposed, which focuses the moving target and estimates its motion parameters without parameter searching, so as to realize fast detection and two-dimensional velocity estimation of moving target. Firstly, each channel is processed separately, the second-order keystone transform is used to correct the range curvature, and the symmetric autocorrelation function in the range frequency domain is calculated. Then, the symmetric autocorrelation function's energy is gathered using chirp-z transform and fast Fourier transform (FFT), so the targets can be detected. Simultaneously, the range migration parameters of each target can be estimated according to the position of the peak, and the azimuth signals of targets are extracted. In order to adapt to the longer aperture time, the azimuth signals are modeled as a fourth-order phase signal. Through phase difference and non-uniform cubic phase function (NUCPF) processing, the coefficients of each order of phase with respect to the slow time can be obtained to estimate the target's relative velocity. Then, for multi-channel joint processing, the azimuth signal is transformed into the Doppler domain, and the interferometric signal is calculated. The phase generated by the interferometric signal is used to estimate the radial velocity of the target.

The structure below is as follows: the characteristics of UWB SAR are presented in Section II; in Section III, the signal model of UWB SAR moving target is constructed; in Section IV, the fast two-dimensional velocity estimation method based on multi-channel SAR data is described in detail; in Section V, the computational complexity of the proposed method is provided; in Section VI, the feasibility of the proposed method is illustrated by simulation experiments, and finally the conclusions are drawn.

II. MULTI-CHANNEL UWB SAR FOR MOVING TARGET INDICATION

This section describes the multi-channel UWB SAR system adopted in this paper. Firstly, the typical parameters of UWB SAR are provided. Then, we discuss the characteristics of UWB SAR. Finally, the geometric configuration of the UWB SAR is given.

The existing UWB SAR system, such as LORA, is equipped with a multi-channel antenna, and the echo data obtained by its dual receivers can be used for the input of the moving target indication processing. The typical UWB SAR parameters are shown in Table 1 [25]. UWB SAR adopts a large beam angle. For example, the maximum accumulation angle of the CARABAS-II system can reach 120°, and the maximum accumulation angle of the P-3 system is 113°.

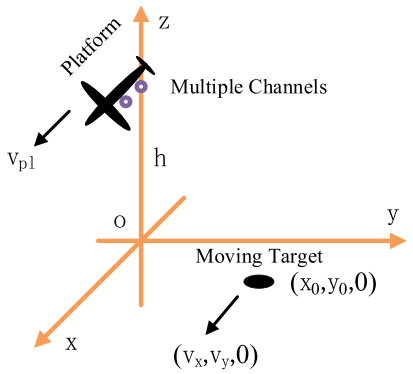

FIGURE 1. Geometric schematic diagram of moving target observation by multi-channel UWB SAR.

TABLE 1. UWB SAR system parameters.

Parameter	Value	Parameter	Value
Power	250 W	System Loss	3 dB
Carrier frequency	400 MHz	Bandwidth	120 MHz
Pulse Width	10 μs	Sampling rate	140 MHz
Pulse repetition frequency	333.3 Hz	Minimum range	13050.8 m
Platform velocity	104 m/s	Platform height	5400 m
Full integration angle	60°	Number of channels	2
Observation time	12 s	Channel interval	1.875 m

The system's large beam angle makes the transmitted signal energy spread in a wide area, and the moving target echo power is very low. Taking the parameters in Table 1 as an example, the SNR of the echo signal calculated according to the radar equation is -17.8 dB. In addition, UWB SAR's wavelength is large, leading to the low resolution in the azimuth direction. The long aperture time can help to improve the azimuthal resolution.

The geometric configuration of a general moving target in UWB SAR is shown in Figure 1. In the coordinate system $oxyz$, o is the platform's projection point on the ground; oz is perpendicular to the horizontal direction; ox points to the direction of the platform's velocity; oy, oz and ox complete the right-hand coordinate system. The platform moves along the x axis with the speed v_{pl} at the height h. The two channels distribute along the flight direction, and the distance between the m^{th} channel and the reference channel is d_m, $m = 1, 2$. The moving target locates at the $(x_0, y_0, 0)$ and moves with a constant speed $(v_x, v_y, 0)$.

III. ECHO SIGNAL MODEL

In order to focus the moving target and estimate its motion parameters, an accurate echo signal model is needed. The signal model derived in this section is based on a series of assumptions. First, the platform moves at a constant speed, and the "stop-go" hypothesis is valid. Second, the target is a point target with uniform linear motion. Based on the geometric model, the moving-target slant range model of the m^{th} channel can be expressed as:

$$R_m(nT_r) = \sqrt{\left(d_m + v_{pl}\cdot nT_r - x_0 - v_x\cdot nT_r\right)^2 + \left(y_0 + v_y\cdot nT_r\right)^2 + h^2} \tag{1}$$

where n is the slow-time index and T_r is the pulse repetition time. The slant range model is determined by the position of the moving target and related to the velocity of the target. Moreover, the defining velocity is the relative velocity of the target to the platform and the radial velocity. Therefore, the slant range model is rewritten and expressed as a function of the relative velocity and radial velocity of the target:

$$R_m(nT_r) = \sqrt{v_{rel}^2\left(nT_r + r_1\frac{\Delta v_m + v_r}{v_{rel}^2}\right)^2 + \rho_m^2} \tag{2}$$

where v_{rel} is the relative velocity of the target related to the platform; v_r is the radial velocity; Δv_m is generated by the delay between channels; ρ_m is the initial slant range of the m^{th} channel, and they can be expressed as:

$$v_{rel}^2 = \left(v_{pl} - v_x\right)^2 + v_y^2 \tag{3}$$

$$v_r = \frac{v_x x_0 + v_y y_0}{r_1} \tag{4}$$

$$\Delta v_m = \frac{v_{pl}\left(d_m - x_0\right) - d_m v_x}{r_1} \tag{5}$$

$$\rho_m^2 = r_m^2 - r_1^2\frac{(\Delta v_m + v_r)^2}{v_{rel}^2} \tag{6}$$

$$r_m^2 = (x_0 - d_m)^2 + y_0^2 + h^2 \tag{7}$$

Then the multi-channel echo signal of the target can be expressed in the form of time-delay and modulation of the transmitted signal. The echo signal model of the m^{th} channel after demodulation can be written as:

$$\begin{aligned} s_{rm}(t_r, n) = {} & \sigma_t \mathrm{rect}\left[\frac{t_r - 2R_m(nT_r)/c}{T_p}\right]\mathrm{rect}\left[\frac{nT_r}{T_a}\right] \\ & \times \exp\left\{j\pi k_r\left(t_r - 2R_m(nT_r)/c\right)^2\right\} \\ & \times \exp\left\{-j4\pi R_m(nT_r)/\lambda\right\} \end{aligned} \tag{8}$$

where t_r is the fast time; σ_t represents the scattering characteristics of the target; T_p is the pulse width; T_a is the synthetic aperture time; k_r is the modulate frequency; λ is the wavelength; c is the speed of light. Then, after range compression we can obtain:

$$\begin{aligned} s_m(t_r, nT_r) = {} & \sigma_t \mathrm{sinc}\left[B_r\left(t_r - \frac{2R_m(nT_r)}{c}\right)\right] \\ & \times \mathrm{rect}\left[\frac{nT_r}{T_a}\right]\exp\left\{-j\frac{4\pi R_m(nT_r)}{\lambda}\right\} \end{aligned} \tag{9}$$

where B_r is the bandwidth.

IV. FAST ALGORITHM FOR TARGET DETECTION AND MOTION PARAMETER ESTIMATION

A. MOVING TARGET DETECTION AND INITIAL RANGE PARAMETER ESTIMATION

Due to the large beam angle and wide wavelength of UWB SAR, moving targets have to face the challenge of severe range migration, low SNR of echoes, and low resolution. Therefore, we only can get better detection performance by accumulating energy on the target. Firstly, we transform the signal shown in (9) into the range frequency domain:

$$s_{1m}(f_r, nT_r) = \sigma_t \mathrm{rect}\left[\frac{f_r}{B_r}\right] \mathrm{rect}\left[\frac{nT_r}{T_a}\right] \times \exp\left\{-j\frac{4\pi (f_r + f_c)}{c} R_m(nT_r)\right\} \quad (10)$$

where f_r is the range frequency and f_c is the operating frequency. The slant range history $R_m(nT_r)$ is in the form of the square root. Therefore, we select a section of the full aperture in azimuth direction for processing. For the selected aperture, the slant range history can be expressed precisely by the fourth-order Taylor expansion. The error of the second-order Taylor expansion is not more than range resolution. The fourth-order Taylor expansion is used to fit the slant range history because of the longer synthetic aperture time than the traditional SAR system. The accurate slant range history is expressed by the square root. For the traditional SAR system, the small beam synthetic aperture time is short, about 1 s or even shorter, and the slant range history can be well fitted by the second-order Taylor expansion. However, for the UWB SAR system, the large beamwidth provides a long observation time, and the traditional second-order expansion will bring intolerable error. Thus, it is necessary to retain higher-order terms to approach the slant range history. However, when the full aperture time (hundreds of seconds) is adopted, in order to ensure the accuracy of the slant range model, the fitting order reaches the eighth or even the ninth order, which significantly increases the complexity of moving target detection and parameter estimation. Therefore, we propose to select only a small section of aperture for imaging and parameter estimation. Considering the influence of resolution, we limit the aperture length to a few seconds. According to system parameters in Table 1, when the aperture time is 12 s, the resolution is 3.92 m. The range errors for different aperture time are shown in Figure 2. Even for the aperture time of 25 s, it can be seen that the fourth-order Taylor expansion of the slant range model meets the focusing requirements, and the second-order Taylor expansion will not exceed 1 range resolution. Then, the slant range history can be expressed as:

$$R_{cut\_m}(nT_r) = r_m + a_1(nT_r) + a_2(nT_r)^2 + a_3(nT_r)^3 + a_4(nT_r)^4 \quad (11)$$

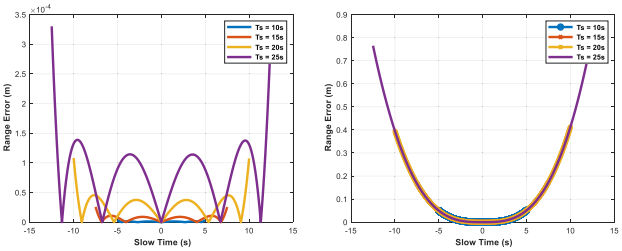

FIGURE 2. The range error of the fourth-order polynomial and the second-order polynomial for different aperture time: (a) the fourth-order polynomial; (b) the second-order polynomial.

where the length of the selected aperture satisfies:

$$T_{a\_sub} < \min\left\{\sqrt[3]{\frac{\rho_r}{a_3}}, \sqrt[5]{\frac{\lambda}{16a_5}}\right\} \quad (12)$$

The coefficients of each order can be expressed as:

$$\begin{aligned} a_1 &= \Delta v_m + v_r \\ a_2 &= \frac{v_{rel}^2 - (\Delta v_m + v_r)^2}{2r_m} \\ a_3 &= -\frac{(\Delta v_m + v_r)\left[v_{rel}^2 - (\Delta v_m + v_r)^2\right]}{2r_m^2} \\ a_4 &= -\frac{\left[v_{rel}^2 - 5(\Delta v_m + v_r)^2\right]\left[v_{rel}^2 - (\Delta v_m + v_r)^2\right]}{8r_m^3} \end{aligned} \quad (13)$$

Then, the signal of the selected aperture can be expressed as:

$$\begin{aligned} &s_{cut\_m}(f_r, nT_r) \\ &= \sigma_t \mathrm{rect}\left[\frac{f_r}{B_r}\right] \mathrm{rect}\left[\frac{nT_r}{T_{a\_sub}}\right] \\ &\quad \times \exp\left\{-j\frac{4\pi (f_r + f_c)}{c}\left[r_m + a_1(nT_r) + a_2(nT_r)^2\right]\right\} \\ &\quad \times \exp\left\{-j\frac{4\pi (f_r + f_c)}{c}\left[a_3(nT_r)^3 + a_4(nT_r)^4\right]\right\} \end{aligned} \quad (14)$$

Thus, it can be seen that there are first-order, second-order, third-order, and fourth-order coupling relationships between the range frequency f_r and slow-time index n. The slant range error generated by the third-order term and the fourth-order term will not exceed range resolution, which will not be considered. In order to eliminate the first-order and second-order coupling, first, we use the second-order Keystone transformation [26] to eliminate the influence of the second-order coupling term, where let:

$$n = \sqrt{\frac{f_c}{f_r + f_c}} n' \quad (15)$$

After the second-order Keystone transformation, we get:

$$\begin{aligned} s_{cut\_m}(f_r, n'T_r) &= \sigma_t \mathrm{rect}\left[\frac{f_r}{B_r}\right] \mathrm{rect}\left[\frac{n_1 T_r}{T_a}\right] \\ &\quad \times \exp\left\{-j\frac{4\pi f_c}{c} R_{cut\_m}(n'T_r)\right\} \\ &\quad \times \exp\left\{-j\frac{4\pi f_r}{c}\left[r_m + \frac{a_1}{2}(n'T_r)\right]\right\} \end{aligned} \quad (16)$$

Then, calculate the bilinear symmetric autocorrelation function [27]:

$$\begin{aligned} &AR_m\left(f_n, n'T_r\right) \\ &= \int_{f_r} s_{cut\_m}\left(f_r + f_n, n'T_r\right) s^*_{cut\_m}\left(f_r - f_n, n'T_r\right) df_r \\ &= A\exp\left\{-j\frac{8\pi f_n}{c}\left[r_m + \frac{a_1}{2}\left(n'T_r\right)\right]\right\} \end{aligned} \tag{17}$$

There is only a linear coupling between f_n and n', so we can use the chirp-z transformation [28] to eliminate the coupling effect:

$$\begin{aligned} &P_m\left(f_n, k\right) \\ &= CZT\left[AR_m\left(f_n, n'T_r\right)\right] \\ &= \sum_{n'=0}^{N_1-1} AR_m\left(f_n, n'T_r\right)\left[e^{-j\pi f_n}\left(e^{-j\frac{2\pi}{N}f_n}\right)^{-k}\right]^{-n_1} \\ &\approx A_p\exp\left\{-j\frac{8\pi f_n}{c}r_m\right\}\mathrm{sinc}\left[\frac{8\pi N f_n}{c}\left(a_1T_r + \frac{k}{2N_1}\right)\right] \end{aligned} \tag{18}$$

The k axis is the Doppler-frequency index axis of the slow-time index n' after chirp z transformation. It can be seen that the targets are aggregated in the direction of the axis k, and then carry out IFFT in the direction of f_n, we can obtain:

$$\begin{aligned} Q_m\left(t_r, k\right) &= \mathrm{IFFT}_{f_n}\left[P_m\left(f_n, k\right)\right] \\ &= A_q\mathrm{sinc}\left\{B_r\left(t_r - \frac{4r_m}{c}\right)\right\} \\ &\quad\times\mathrm{sinc}\left[\frac{8\pi N_1 f_n}{c}\left(a_1T_r + \frac{k}{2N_1}\right)\right] \end{aligned} \tag{19}$$

The target's energy is accumulated, which can realize the target detection, and the peak value appears at the position $\left(4\frac{r_m}{c}, -2a_1NT_r\right)$. The estimated parameters can be used to compensate the range migration of the target. When there are multiple targets, the cross term between targets will not accumulate [27], and different targets will be focused at different positions due to different locations and speeds. According to this feature, multiple targets can be detected, and their range migration parameters can be estimated respectively. According to the estimated parameters, the reference function is constructed as:

$$s_{ref\_m}\left(f_r, nT_r\right) = \exp\left\{j\frac{2\pi f_r}{c}a_1\left(nT_r\right)\right\} \tag{20}$$

We use the reference function to compensate the signal in (16) to achieve the range migration correction of the target:

$$\begin{aligned} s_{2m}\left(t_r, nT_r\right) &= \mathrm{IFFT}_{f_r}\left[s_{cut\_m}\left(f_r, nT_r\right)s_{ref\_mq}\left(f_r, nT_r\right)\right] \\ &= \sigma_t\mathrm{rect}\left[\frac{nT_r}{T_a}\right]\mathrm{sinc}\left[B_r\left(t_r - \frac{2r_m}{c}\right)\right] \\ &\quad\times\exp\left\{-j\frac{4\pi f_c}{c}R_{cut\_m}\left(nT_r\right)\right\} \end{aligned} \tag{21}$$

According to the estimated parameters, the signal at $t_r = 2r_m/c$ is extracted to obtain the target signal in the azimuth direction:

$$s_{a\_m}\left(nT_r\right) = \sigma_t\mathrm{rect}\left[\frac{nT_r}{T_a}\right]\exp\left\{-j\frac{4\pi f_c}{c}R_{cut\_m}\left(nT_r\right)\right\} \tag{22}$$

B. MOTION PARAMETER ESTIMATION

1) RELATIVE VELOCITY ESTIMATION OF MOVING TARGET

In order to achieve the estimation of each target's motion parameters, we process the signal in the azimuth direction. The signal can be approximated by the four-order phase signal. In order to convert the signal into the third-order phase signal, first of all, we use the phase difference for the reduced-order processing:

$$\begin{aligned} &PD_m\left[n; p\right] \\ &= s_{a\_m}\left(T_r\left(n+p\right)\right)s^*_{a\_m}\left(T_r\left(n-p\right)\right) \\ &= \exp\left\{-j\frac{8\pi pT_r}{\lambda}\left[a_1 + a_3p^2T_r^2 + \left(2a_2 + 4a_4p^2T_r^2\right)nT_r\right]\right\} \\ &\quad\times A_{pd}\exp\left\{-j\frac{8\pi pT_r}{\lambda}\left[3a_3\left(nT_r\right)^2 + 4a_4\left(nT_r\right)^3\right]\right\} \end{aligned} \tag{23}$$

For the reference channel signal, NUCPF can be expressed as [29]:

$$\begin{aligned} &NUCPF\left(n, \Omega\right) \\ &= \sum_k PD_1\left(n + \sqrt{Ck}\right)PD_1\left(n - \sqrt{Ck}\right)e^{j\Omega T_r^2Ck} \\ &= PD_1^2\left(n\right)\sum_k\exp\left\{-j\frac{4\pi pT_r^3}{\lambda}\left[\left(6a_3 + 24a_4T_rn\right) - \Omega\right]Ck\right\} \end{aligned} \tag{24}$$

We select two different time slices, i.e. n_1, n_2, and detect the peak values of their $|NUCPF\left(n, \Omega\right)|$ to obtain $\hat{\Omega}_1, \hat{\Omega}_2$, and thus we obtain the equations of a_3, a_4, and we solve them to get:

$$\begin{aligned} \hat{a}_3 &= \left(\hat{\Omega}_1n_2 - \hat{\Omega}_2n_1\right)/6\left(n_2 - n_1\right) \\ \hat{a}_4 &= \left(\hat{\Omega}_1 - \hat{\Omega}_2\right)/24T_r\left(n_1 - n_2\right) \end{aligned} \tag{25}$$

We use the $\hat{a}_3, \hat{a}_4$ to demodulate the signal. The signal after demodulation can be expressed as:

$$\begin{aligned} s_{PD\_de}\left(nT_r\right) &= A_{pd}^2\exp\left\{-j\frac{4\pi pT_r}{\lambda}\left[a_1 + a_3T_r^2p^2\right]\right\} \\ &\quad\times\exp\left\{-j\frac{4\pi pT_r}{\lambda}\left[2\left(a_2T_r + 2a_4T_r^3p^2\right)n\right]\right\} \end{aligned} \tag{26}$$

The peak of the spectrum of $s_{PD\_de}\left(nT_r\right)$ will appear at $f = -\frac{4pT_r^2}{\lambda}\left(a_2 + 2a_4T_r^2\tau_1^2\right)$, and it can be estimated that:

$$\hat{a}_2 = -\frac{\lambda}{4pT_r^2}\arg\max_f\left|\mathrm{FFT}\left[s_{PD\_de}\left(nT_r\right)\right]\right| - 2\hat{a}_4T_r^2p^2 \tag{27}$$

At this point, the second order a_2 of the target has been estimated. According to (13), the relative velocity v_{rel} can be calculated as:

$$v_{rel}^2 = a_2 r_1 \tag{28}$$

2) RADIAL VELOCITY ESTIMATION OF MOVING TARGET

A single channel cannot estimate the two-dimensional velocity of the target. Therefore, we use the dual-channel data to obtain the relative radial velocity of the target so as to achieve the target positioning. Firstly, we transform the signal (22) in the azimuth direction into the Doppler domain. Consider that the distance between channels and the length of the aperture is much smaller than the slant range, then

$$\begin{aligned} &s_{a\_m}(nT_r) \\ &\approx \sigma_t \mathrm{rect}\left[\frac{nT_r}{T_a}\right] \exp\left\{j\frac{4\pi d_m}{\lambda v_{pl}} v_r\right\} \\ &\quad \exp\left\{-j\frac{4\pi}{\lambda}\sqrt{v_{rel}^2\left(nT_r + \frac{d_m}{v_{pl}} + \frac{r_1 v_r - x_0 v_{pl}}{v_{rel}^2}\right)^2 + r_1^2}\right\} \end{aligned} \tag{29}$$

Then, the azimuth signal in the frequency domain can be expressed as:

$$\begin{aligned} s_{a\_m}(f_a) = \mathrm{FFT}\left[s_A(nT_r)\right] \exp\left\{j\frac{4\pi d_m}{\lambda v_{pl}} v_r\right\} \\ \times \exp\left\{-j2\pi f_a \cdot \frac{d_m}{v_{pl}}\right\} \end{aligned} \tag{30}$$

where:

$$\begin{aligned} &s_A(nT_r) \\ &= \sigma_t \mathrm{rect}\left[\frac{nT_r}{T_a}\right] \\ &\quad \times \exp\left\{-j\frac{4\pi}{\lambda}\sqrt{v_{rel}^2\left(nT_r + \frac{r_1 v_r - x_0 v_{pl}}{v_{rel}^2}\right)^2 + r_1^2}\right\} \end{aligned} \tag{31}$$

The interferometric signal between different channels is:

$$\begin{aligned} I(f_a) &= s_{a\_1}(f_a)\, s_{a\_2}^*(f_a) \\ &= A_I \exp\left\{j\frac{4\pi (d_1 - d_2)}{\lambda v_{pl}} v_r\right\} \exp\left\{-j2\pi f_a \frac{(d_1 - d_2)}{v_{pl}}\right\} \end{aligned} \tag{32}$$

where d_m is the distance between the m^{th} channel and the reference channel. Then, the second phase of (32) can be compensated according to the system parameters. After the compensation, the target's radial velocity can be estimated as:

$$v_r = \frac{\lambda v_{pl}}{4\pi (d_1 - d_2)}\varphi \tag{33}$$

Based on the above analysis, referring to the existing framework of robust parameter estimation system [30]–[32], the flow chart of a fast two-dimensional velocity estimation method for multi-channel UWB SAR is shown in Figure 3. The detailed treatment process is as follows:

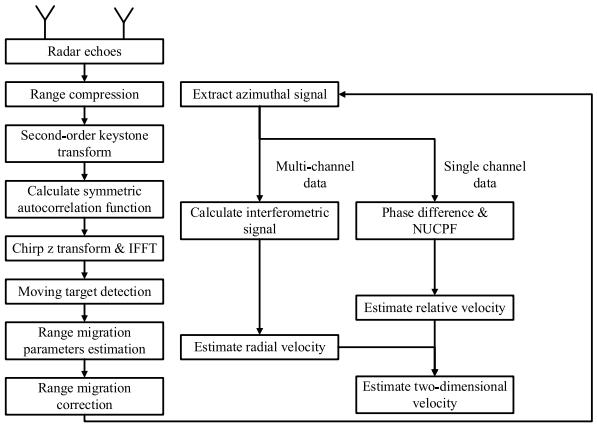

FIGURE 3. Flow chart of fast two-dimensional velocity estimation method for moving target in multi-channel UWB SAR.

Step 1: carry out range compression and second-order keystone transform for an echo signal to realize range curvature correction.

Step 2: calculate the symmetric autocorrelation function in the range frequency domain, and use chirp z transformation and IFFT transformation to realize the energy accumulation of the moving target.

Step 3: detect the target and estimate the range migration parameters according to the peak value location, which is used for range migration correction and azimuth signal extraction.

Step 4: transform the dual-channel data into the Doppler domain and calculate the interferometric signal. The target radial velocity can be estimated by the phase.

Step 5: perform phase difference and NUCPF processing on the reference channel data to estimate the relative velocity.

Step 6: the two-dimensional velocity of the target is obtained by combining the radial velocity, and the target's relative velocity.

V. COMPUTATIONAL COMPLEXITY ANALYSIS

In order to show the computational complexity (CC) of the proposed method, it is compared with the representative UWB SAR parameter estimation algorithm, namely the method based on normalized relative speed (NRS) [7], [8]. Suppose the number of range cells and the number of pulses are N_r and N_a respectively, and the search times of target slant range, azimuth position, radial velocity, and relative velocity are N_{x_r}, N_{x_a}, N_{v_r}, and N_γ respectively. For the method based on NRS, the unknown parameters need to be searched in four dimensions to realize the coherent integration of moving targets entirely. Thus, the CC of the method based on NRS is $O\left(N_{v_r} N_\gamma N_{x_r} N_{x_a} N_r N_a\right)$. For the technique proposed in this paper, the CC can be obtained according to the main steps. The second-order Keystone transformation's CC is $O\left(N_a N_r \log_2 N_a\right)$, the symmetric autocorrelation function's CC is $O\left(N_r^2 N_a\right)$, the Chirp Z and IFFT's CC

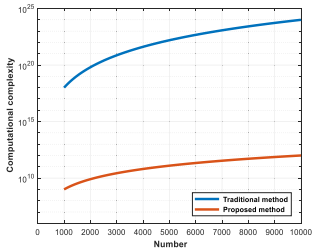

FIGURE 4. Computational complexity comparison.

TABLE 2. Single moving target parameters.

Parameter	x (m)	y (m)	v_r (m/s)	v_{rel} (m/s)
Value	1288	11500	9.8125	96.5194

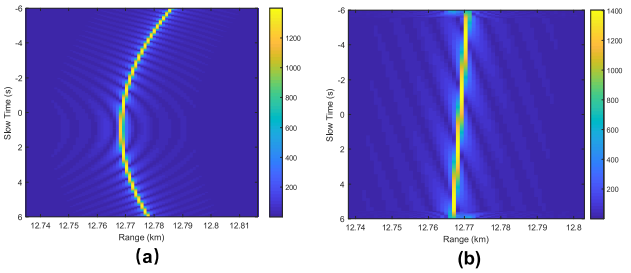

FIGURE 5. (a) The echo signal after range compression. (b) The results after the second-order keystone transformation.

is $O\left(N_a N_r \left(\log_2 N_a + \log_2 N_r\right)\right)$, the radial velocity estimation's CC is $O\left(N_a \log_2 N_a\right)$, and the NUCPF processing's CC is $O\left(N_a \log_2 N_a\right)$. Thus, the CC of the whole process is $O\left(N_a N_r^2\right)$. Assuming that $N_a = N_r = N_{x_r} = N_{x_a} = N_{v_r} = N_\gamma = N$. The CC under different points is given in Figure 4. It can be seen that the CC of the proposed algorithm is significantly lower than that of the traditional algorithm, and when $N = 2000$, the CC of the traditional algorithm is approximately 10^{10} times that of the proposed algorithm. Thus, the superiority of the proposed algorithm in CC can be proved.

VI. SIMULATION EXPERIMENT VERIFICATION

In this section, UWB SAR simulation data are used to verify the effectiveness of the proposed method. Radar parameters are shown in Table 1. Our simulation experiments are divided into two parts. Firstly, the single target's detection and parameters estimation is simulated. Then, processing with multiple targets is also conducted.

A. SINGLE MOVING TARGET

The parameters of the single moving target can be seen in Table 2. When there is no noise, the echo signal after range compression can be seen in Figure 5 (a), in which the target has severe range curvature. It is obvious that its range migration is much more severe and spans several range cells. It results from the increase of synthetic aperture time. From the simulation results, the length of range migration is 17.50 m and spans 14 range cells. Thus, the impact of

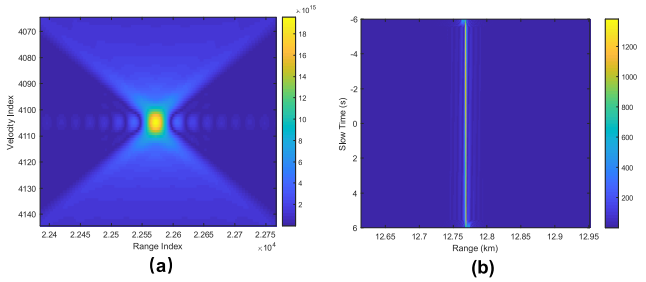

FIGURE 6. (a) The symmetric autocorrelation function after the accumulation. (b) The results after the range migration correction.

range migration has to be considered in processing. After the second-order keystone transformation, as seen in Figure 5 (b), the range curvature has been corrected, and the trajectory of the target in the image is a line. The second-order Keystone transformation is used to correct the quadratic migration. After the transformation, the range curvature has been removed, and the residual range migration is only caused by the range walking.

Then, the symmetric autocorrelation function in the range frequency is calculated, and after chip-z and IFFT processing, the result is shown in Figure 6 (a). It can be seen that the moving target has been accumulated, and there is a peak. The peak position implies the range and velocity of the target, and the parameters can be used to correct range migration. In the processing, the coupling terms between the range and linear term have been removed by chirp z transformation. Then, the target can realize energy accumulation both in the range axis and velocity axis. The location of the target is determined by its shortest slant range and speed. From the results, it can be estimated that the slant range of the target is 12767.68 m, and the deviation is 0.46 m, which is less than a range resolution cell (1.25 m). The target's shortest slant range can be estimated accurately. Moreover, the estimated residual range walking is 4.75 m, and the deviation is 0.6 m, which is also smaller than a range resolution cell. Thus, the estimated parameters can be used to correct the range migration and ensure that the target does not exceed a range resolution cell, which leads to the results in Figure 6 (b). After the range migration correction, the result is presented in Figure 6 (b). The coupling between the slow time and the range has been removed, and the target's azimuth signal can be extracted.

Next, the azimuth signal is processed by phase difference and NUCPF. The second-order phase term's coefficient can be obtained to estimate the relative velocity, which is 96.5088 m/s. Then, the interferometric signal is calculated to estimate the radial velocity, which is 9.7966 m/s. Thus, the two-dimensional velocities are estimated accurately and the accuracies of relative velocity and radial velocity are 0.011 m/s and 0.016 m/s, respectively. The proposed method estimates the parameters by accumulating the target's energy and exploiting the peak position to complete parameter estimation. Because of the impacts of resolution and the discrete data, there is a bias between the estimated parameter and the

TABLE 3. Estimation results for different SNR.

SNR	v_r (m/s)	v_{rel} (m/s)	Error on v_r (m/s)	Error on v_{rel} (m/s)
Without noise	9.7966	96.5088	0.016	0.011
-10 dB	9.7891	96.5931	0.074	0.023
-20 dB	9.7988	96.4210	0.014	0.098
-30 dB	9.9324	98.0580	0.1200	1.5386

TABLE 4. Multiple moving targets parameters.

Parameter	x (m)	y (m)	v_r (m/s)	v_{rel} (m/s)
Target 1	1288	11500	9.8125	96.5194
Target 2	1288	11550	5.6088	102.1763
Target 3	1288	11800	-2.6318	94.0851
Target 4	1288	11800	0.3951	100.0000
Target 5	1288	11900	2.8403	112.0714
Target 6	1288	11950	6.8643	108.2959

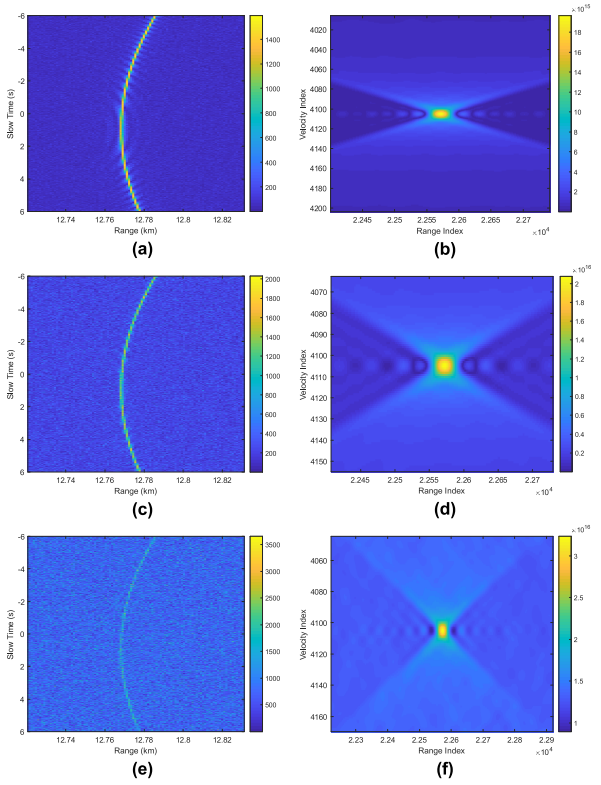

FIGURE 7. The echo signal after range compression and the symmetric autocorrelation function after the accumulation: (a) and (b) are the results when SNR is -10 dB; (c) and (d) are the results when SNR is -20 dB; (e) and (f) are the results when SNR is -30 dB.

actual value. The errors refer to an individual trial. Therefore, they are the scope to show an example of performance rather than an accuracy evaluation.

Finally, different SNRs of the echoes have been simulated. The echoes' SNRs are set to be -10 dB -20 dB, and -30 dB, respectively. The echo signals after range compression are shown in Figure 7 (a), (c), and (e). Because of the reduction

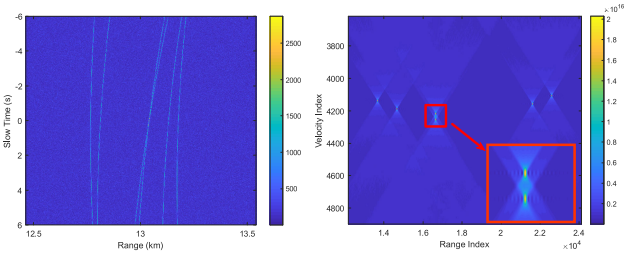

FIGURE 8. (a) Result of range compression of echo signal. (b) the symmetric autocorrelation function after the accumulation.

TABLE 5. Estimation results of multiple moving targets parameters.

Parameter	v_r (m/s)	v_{rel} (m/s)	Error on v_r (m/s)	Error on v_{rel} (m/s)
Target 1	9.7870	96.6155	0.026	0.096
Target 2	5.5141	101.8120	0.095	0.364
Target 3	-2.5999	94.1724	0.032	0.087
Target 4	0.2071	100.7298	0.188	0.270
Target 5	2.7687	111.7834	0.078	0.288
Target 6	6.8177	108.5457	0.047	0.250

of SNR, the targets cannot be seen clearly in the image, especially for the SNR of -30 dB, which means the accumulation before the detection is necessary. The symmetric autocorrelation function in the range frequency after chip-z and IFFT processing is shown in Figure 7 (b), (d), and (f). The target has been accumulated and can be detected even with an SNR of -30 dB. After the estimation, the relative velocities and the radial velocities are shown in Table 3. Under the influence of noise, in the NUCPF processing and interference signal processing, the target's position after energy accumulation will deviate, so the estimation error will also increase with the rise of noise energy. From the results, the proposed method is still effective when the SNR is low. When the SNR is -30 dB, the errors of the relative velocity and radial velocity both increase obviously. The errors do not exceed 0.1 m/s when the SNR is not less than -20 dB.

B. MULTIPLE MOVING TARGETS

There are six moving targets set in the scene. The targets' position and speed parameters are shown in Table 4, and the SNR of the target is -10 dB.

The echo signal after range compression is shown in Figure 8 (a). It can be seen that the target is impacted by noise. After range processing, each target's energy is accumulated, as shown in Figure 8 (b). The horizontal axis represents the shortest slant range of the target, while the vertical axis represents the first-order coefficient of the slant range, which is mainly determined by the target speed. It can be seen from the figure that due to the energy accumulation, the target has a high SNR, which can be used to achieve target detection. In addition, target 1, target 2, target 3, target 5, and target 6 are separated in different range cells. Target 3 and target 4 appear in the same range cell, but they are separated in the velocity dimension due to their different velocities. In short,

the target will be separated in the plane due to the difference of position and velocity so that the multi-target detection can be realized.

Next, the azimuth signal and multi-channel signal are processed to estimate the target's velocity parameters, including relative velocity and radial velocity. The estimation results are shown in Table 5. Compared with the parameters in Table 4, the root mean square error of radial velocity is 0.094 m/s, and the root mean square error of relative velocity is 0.247 m/s. Thus, the proposed method is effective for multiple targets, and the two-dimensional velocities can be estimated accurately.

VII. CONCLUSION

In this paper, a fast two-dimensional velocity estimation method for multi-channel UWBSAR is proposed, in which the target detection can be detected and its motion parameters are estimated without using parameter search. Firstly, the second-order keystone transform, symmetric autocorrelation function in the range frequency domain, chirp Z transform and fast Fourier transform are used to process the echo signal to realize the energy accumulation of the target, detect the target and estimate the range migration parameters of the target. Then, the range migration correction is carried out for each target, and the azimuth signal is extracted. The azimuth signal is processed by NUCPF to obtain the coefficients of each order of slant range history to realize the relative velocity estimation. Next, the target's radial velocity is estimated by using the phase difference of multi-channel in the Doppler domain. Finally, the algorithm's feasibility is demonstrated by simulation experiments. The proposed method can estimate the two-dimensional velocity accurately when the SNR is not less than -20 dB.

REFERENCES

[1] M. Y. Chua, V. C. Koo, H. S. Lim, and J. T. Sri Sumantyo, "Phase-coded stepped frequency linear frequency modulated waveform synthesis technique for low altitude ultra-wideband synthetic aperture radar," *IEEE Access*, vol. 5, pp. 11391–11403, 2017.

[2] M. I. Pettersson, "Moving target detection in wide band SAR," in *Proc. CIE Int. Conf. Radar*, 2001, pp. 614–618.

[3] M. I. Pettersson, "Detection of moving targets in wideband SAR," *IEEE Trans. Aerosp. Electron. Syst.*, vol. 40, no. 3, pp. 780–796, Jul. 2004.

[4] L. M. H. Ulander, M. Blom, B. Flood, P. Follo, P.-O. Frolind, A. Gustavsson, T. Jonsson, B. Larsson, D. Murdin, M. Pettersson, U. Raaf, and G. Stenstrom, "Development of the ultra-wideband LORA SAR operating in the VHF/UHF-band," in *Proc. IGARSS. IEEE Int. Geosci. Remote Sens. Symp.*, vol. 7, Jul. 2003, pp. 4268–4270.

[5] V. T. Vu, T. K. Sjogren, M. I. Pettersson, H.-J. Zepernick, and A. Gustavsson, "Experimental results on moving target detection by focusing in UWB low frequency SAR," in *Proc. IET Int. Conf. Radar Syst.*, 2007, pp. 1–5.

[6] M. I. Pettersson, "Four-dimensional discretization for detection of moving objects in wide band SAR," in *Proc. Eur. Radar Conf.*, Oct. 2007, pp. 79–82.

[7] T. K. Sjogren, V. T. Vu, M. I. Pettersson, H.-J. Zepernick, and A. Gustavsson, "Speed estimation experiments for ground moving targets in UWB SAR," in *Proc. IET Int. Conf. Radar Syst.*, 2007, pp. 1–5.

[8] T. K. Sjogren, V. T. Vu, M. I. Pettersson, A. Gustavsson, and L. M. H. Ulander, "Moving target relative speed estimation and refocusing in synthetic aperture radar images," *IEEE Trans. Aerosp. Electron. Syst.*, vol. 48, no. 3, pp. 2426–2436, Jul. 2012.

[9] V. T. Vu, T. K. Sjogren, and M. I. Pettersson, "Moving target detection by forcusing for frequency domain algorithms in UWB low frequency SAR," in *Proc. IGARSS-IEEE Int. Geosci. Remote Sens. Symp.*, 2008, pp. I-161–I-164.

[10] V. T. Vu, T. K. Sjogren, and M. I. Pettersson, "Ultrawideband chirp scaling algorithm," *IEEE Geosci. Remote Sens. Lett.*, vol. 7, no. 2, pp. 281–285, Apr. 2010.

[11] V. T. Vu, T. K. Sjogren, M. I. Pettersson, and P. A. C. Marques, "Application of the moving target detection by focusing technique in civil traffic monitoring," in *Proc. IEEE Int. Geosci. Remote Sens. Symp.*, Jul. 2010, pp. 4118–4121.

[12] V. Vu, M. Pettersson, and T. Sjogren, "Local detection of moving target by focusing in SAR images," in *Proc. IEEE Radar Conf. (RadarConf)*, May 2016, pp. 1–6.

[13] V. T. Vu, "Local detection of moving targets in SAR image based on NRS hypotheses," *IEEE Trans. Geosci. Remote Sens.*, vol. 56, no. 10, pp. 6101–6110, Oct. 2018.

[14] V. T. Vu, T. K. Sjogren, M. I. Pettersson, A. Gustavsson, and L. M. H. Ulander, "Detection of moving targets by focusing in UWB SAR—Theory and experimental results," *IEEE Trans. Geosci. Remote Sens.*, vol. 48, no. 10, pp. 3799–3815, Oct. 2010.

[15] V. T. Vu, T. K. Sjogren, and M. I. Pettersson, "Fast detection of moving targets by focusing in UWB low frequency SAR," in *Proc. IEEE Radar Conf.*, May 2009, pp. 1–5.

[16] J. Yang, X. Huang, H. Thompson, T. Jin, and Z. Zhou, "Low-frequency ultra-wideband synthetic aperture radar ground moving target imaging," *IET Radar, Sonar Navigat.*, vol. 5, no. 9, pp. 994–1001, Dec. 2011.

[17] M. Soumekh, "Moving target detection in foliage using along track monopulse synthetic aperture radar imaging," *IEEE Trans. Image Process.*, vol. 6, no. 8, pp. 1148–1163, Aug. 1997.

[18] M. I. Pettersson, "Extraction of moving ground targets by a bistatic ultra-wideband SAR," *IEE Proc.-Radar, Sonar Navigat.*, vol. 148, no. 1, pp. 35–40, Feb. 2001.

[19] Z. Hong, H. Xiaotao, C. Yulin, and Z. Zhimin, "Single-channel UWB SAR ground moving targets detection method using change detection based on single-pass sub-aperture images," in *Proc. 1st Asian Pacific Conf. Synth. Aperture Radar*, Nov. 2007, pp. 266–270.

[20] V. T. Vu, T. K. Sjogren, and M. I. Pettersson, "Fast detection of moving targets by focusing in UWB low frequency SAR," in *Proc. Eur. Radar Conf.*, May 2009, pp. 218–221.

[21] H. Zhou, Y. Chang, X. Huang, and Z. Zhou, "Moving target detection and velocity estimation using multiple subband DPCA and ATI method for triple-channel UWB SAR," in *Proc. 9th Int. Conf. Signal Process.*, Oct. 2008, pp. 2653–2656.

[22] Y.-L. Chang, H. Zhou, X.-T. Huang, and Z.-M. Zhou, "The representation of moving targets in multi-channel UWB SAR images and it's application in the generalization of image domain GMTI methods," in *Proc. 9th Int. Conf. Signal Process.*, Oct. 2008, pp. 2525–2528.

[23] Y.-L. Chang, H. Zhou, X.-T. Huang, and Z.-M. Zhou, "Moving target focusing and parameter estimation based on ROI of multi-channel UWB SAR images," in *Proc. 9th Int. Conf. Signal Process.*, Oct. 2008, pp. 2529–2532.

[24] H. Zhou, M. Zhu, Y. Chang, X. Huang, and Z. Zhou, "Performance analysis of subband STAP for UWB SAR sparse array," in *Proc. IET Int. Radar Conf.*, 2009, pp. 1–5.

[25] H. Hellsten, L. M. H. Ulander, A. Gustavsson, and B. Larsson, "Development of VHF CARABAS II SAR," *Proc. SPIE*, vol. 2747, pp. 48–60, Jun. 1996.

[26] D. Kirkland, "Imaging moving targets using the second-order keystone transform," *IET Radar, Sonar Navigat.*, vol. 5, no. 8, pp. 902–910, Oct. 2011.

[27] Z. Jiancheng, S. Tao, Z. Jibin, and H. Xuehui, "Novel fast coherent detection algorithm for radar maneuvering target with jerk motion," *IEEE J. Sel. Topics Appl. Earth Observ. Remote Sens.*, vol. 10, no. 5, pp. 1792–1803, May 2017.

[28] L. Rabiner, R. Schafer, and C. Rader, "The chirp z-transform algorithm," *IEEE Trans. Audio Electroacoust.*, vol. AU-17, no. 2, pp. 86–92, Jun. 1969.

[29] D. Li, C. Zhang, H. Ma, H. Liu, J. Su, and Q. Liu, "An efficient SAR ground moving target refocusing method based on PPFFT and coherently integrated CPF," *IEEE Access*, vol. 7, pp. 114102–114115, 2019.

[30] Y. Chen, Y. Yao, and Y. Zhang, "A robust state estimation method based on SOCP for integrated electricity-heat system," *IEEE Trans. Smart Grid*, vol. 12, no. 1, pp. 810–820, Jan. 2021.

[31] Y. Chen, J. Ma, P. Zhang, F. Liu, and S. Mei, "Robust state estimator based on maximum exponential absolute value," *IEEE Trans. Smart Grid* vol. 8, no. 4, pp. 1537–1544, Jul. 2017.
[32] Y. Chen, F. Liu, S. Mei, and J. Ma, "A robust WLAV state estimation using optimal transformations," *IEEE Trans. Power Syst.*, vol. 30, no. 4, pp. 2190–2191, Jul. 2015.

TONGXIN DANG was born in Shijiazhuang, China, in 1977. He received the B.S. and M.S. degrees from Zhengzhou Information Science and Technology Institute, in 2000 and 2005, respectively. He is currently pursuing the Ph.D. degree with Strategic Support Force Information Engineering University for Radar Signal Processing. His research interests include SAR and ISAR imaging.

YIN XIANG was born in Hubei, China, in 1981. He received the B.S. degree in electronic engineering from the University of Science and Technology of China, Hefei, China, in 2004, and the Ph.D. degree in electronic engineering from the University of Chinese Academy of Sciences, Beijing, China, in 2010. From 2010 to 2012, he held a postdoctoral position at the Institute of Electronics, Chinese Academy of Sciences, Beijing. From 2013 to 2016, he was an Engineer of Radar System with Radar and Electronic Technology Company, Beijing. Since 2017, he has been an Assistant Researcher with the Beijing Institute of Technology, Beijing. He is currently an Assistant Researcher with the Beijing Institute of Technology Chongqing Innovation Center, Chongqing, China. His research interests include microwave imaging, antenna and propagation, sparse signal processing, and radar systems.